

ON THE NON-ORIENTABLE 3- AND 4-GENERA OF A KNOT: CONNECTIONS AND COMPARISONS

JULIA KNIHS, JEANETTE PATEL, THEA RUGG, AND JOSHUA M. SABLOFF

ABSTRACT. We define a new quantity, the Euler-normalized non-orientable genus, to connect a variety of ideas in the theory of non-orientable surfaces bounded by knots. This quantity is used to reframe non-orientable slice-torus bounds on the non-orientable 4-genus, to bound below the Turaev genus as a measure of distance to an alternating knot, and to understand gaps between the 3- and 4-dimensional non-orientable genera of pretzel knots. Further, we make connections to essential surfaces in knot complements and the Slope Conjecture.

CONTENTS

1. Introduction	1
2. Spanning Surfaces in 3 Dimensions	6
3. Fillings in 4 Dimensions	14
4. Euler-Normalized Genus Agreements: Alternating Knots and the Turaev Genus	18
5. Ordinary Genus Gaps: Pretzel Knots	22
6. Euler-Normalized Genus Gaps: Slice Pretzel Knots	25
7. Euler-Normalized Genus Gaps: Connected Sums	33
References	34

1. INTRODUCTION

This paper seeks to tie together several threads in the theory of non-orientable surfaces bounded by knots using a new quantity called the Euler-normalized non-orientable genus of a knot. This quantity has both 3- and 4-dimensional versions. We investigate this quantity in several settings: first, we reframe the meaning of non-orientable slice torus bounds on the non-orientable 4-genus. Second, we show that the quantity vanishes on alternating knots and, in fact, yields a lower bound on the Turaev genus. Finally, we use it to understand gaps between the 3- and 4-dimensional non-orientable genus for pretzel knots and connected sums. Along the way, we will suggest connections to essential surfaces, the colored Jones polynomial, and the Slope Conjecture.

Date: February 16, 2026.

1.1. Non-Orientable Genera of a Knot. To define the Euler-normalized non-orientable genera of a knot $K \subset S^3$, we begin by setting notation. A compact smooth embedded surface $F \subset S^3$ with $\partial F = K$ is a **spanning surface** of K . Let $\mathcal{F}_3(K)$ be the set of all spanning surfaces of K . Define the **non-orientable 3-genus**, or **crosscap number**, of K to be

$$\gamma_3(K) = \min\{b_1(F) : F \in \mathcal{F}_3(K)\}.$$

This quantity was first introduced by Clark [9], and has been computed for torus knots [42], 2-bridge knots [25], pretzel knots [27] and others; further, there exists an algorithm for determining γ_3 for alternating knots [2] and more general algorithms that use normal surface theory [7].

Similarly, a compact smooth properly embedded surface $F \subset B^4$ with $\partial F = K$ is a **filling** of K . Let $\mathcal{F}_4(K)$ be the set of all fillings of K . The (smooth) **non-orientable 4-genus** of a knot K is

$$\gamma_4(K) = \min\{b_1(F) : F \in \mathcal{F}_4(K)\}.$$

Note that $\gamma_4(K) \leq \gamma_3(K)$. The non-orientable 4-genus was first studied by Viro [44] and Yasuhara [45]. Efforts at understanding γ_4 use tools from algebraic topology [17, 19] and from modern invariants such as Heegaard Floer homology [3, 5, 6, 18, 38], Khovanov homology [4], and gauge theory [11]; see [40] and Section 3 below for a framework for many modern invariants.

A non-orientable filling F has a second interesting homological invariant beyond its first Betti number, namely the Euler class of its normal bundle, termed the **normal Euler number** $e(F) \in 2\mathbb{Z}$. The normal Euler number of a spanning surface is defined to be the normal Euler number of the filling that results from pushing the interior of the spanning surface into B^4 ; note that the normal Euler number of a spanning surface is the *negative* of its **boundary slope**. See Sections 2 and 3 for the precise definitions of the normal Euler number, boundary slope, and other foundational concepts.

We are now ready to define our central object of study, the Euler-normalized non-orientable genus. For a spanning surface or filling F of K , define its **Euler-normalized first Betti numbers** to be

$$\Gamma^\pm(F) = b_1(F) \pm \left(\sigma(K) - \frac{1}{2}e(F) \right),$$

where $\sigma(K)$ is the signature of K .

A key feature of $\Gamma^+(F)$ (resp. $\Gamma^-(F)$) is that it is invariant under the **addition of a +twisted band** (resp. a --twisted band), as in Figure 1. Such an addition raises the first Betti number by 1 and changes the normal Euler number by ± 2 , while leaving the isotopy class of the boundary unchanged. We denote by $\text{tw}_\pm(F)$ the addition of a positive or negative twisted band to F . This feature of $\Gamma^\pm(F)$ is the origin of the moniker “Euler-normalized”.

As we shall see in Section 3.3, a second important feature of the Euler-normalized first Betti number is that it is non-negative, and hence it makes sense to minimize over all spanning surfaces or fillings.

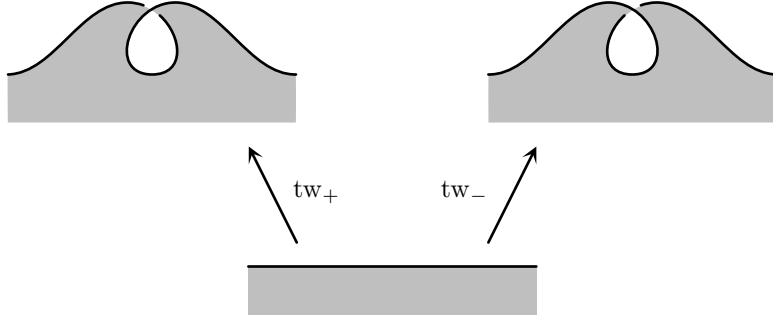


FIGURE 1. The addition of \pm -twisted band to a spanning surface or filling F of K raises the first Betti number by 1 and changes the normal Euler number by ± 2 , but leaves invariant $\Gamma^\pm(F)$ and the isotopy class of the boundary. The sign convention for the normal Euler number means that the sign of the crossing is the opposite of the sign of the twist.

Definition 1.1. The **\pm -Euler-normalized non-orientable n -genus** of a knot K , for $n = 3, 4$, is defined to be

$$\hat{\gamma}_n^\pm(K) = \min\{\Gamma^\pm(F) : F \in \mathcal{F}_n(K)\}.$$

We also define the **average Euler-normalized n -genus** of K to be

$$\bar{\gamma}_n(K) = \frac{1}{2} (\hat{\gamma}_n^+(K) + \hat{\gamma}_n^-(K)).$$

We will argue below that all of these quantities are fundamentally different from the (ordinary) non-orientable genera.

1.2. Inspiration from Geography Questions. The definition of the Euler-normalized non-orientable genus arose from explorations into Allen's geography problem for the non-orientable 4-genus [3]. For a knot K , Allen asked for a description of the set $R_4(K)$ of possible pairs (e, b) realized by the normal Euler number and first Betti number, respectively, of a filling of K . We may define $R_3(K)$ similarly; note that $R_3(K) \subset R_4(K)$. As depicted in Figure 2, the set $R_*(K)$ is constrained by the Gordon-Litherland signature bound, with points of $R(K)$ lying in the wedge

$$W_\sigma = \left\{ b \geq \frac{1}{2} |e - 2\sigma(K)| \right\} \subset \mathbb{Z}^2.$$

In the geography diagram, we may read off $\gamma_n(K)$ as the lowest height of a point in $R_n(K)$, whereas $\hat{\gamma}_n^+(K)$ (resp. $\hat{\gamma}_n^-(K)$) is the minimum vertical distance from $R_n(K)$ to the upward-sloping (resp. downward-sloping) boundary of W_σ . See Sections 2.1, 3.1, and 3.3, below, for a more detailed discussion.

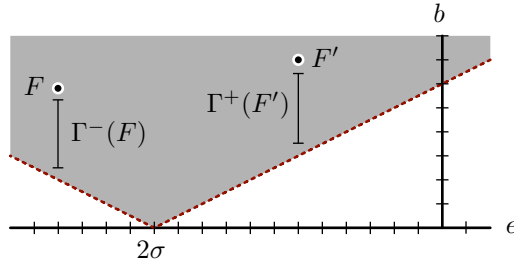


FIGURE 2. The geography $R_*(K)$ is constrained by the Gordon-Litherland signature bound. The Euler-normalized first Betti number measures the vertical distance from the (e, b) coordinates of a surface to the signature bound.

The geography perspective leads to a reframing of many non-orientable slice-torus bounds. For example, we may reinterpret the Heegaard-Floer v bound on the non-orientable 4-genus of [38] as in the following theorem, which we shall prove in Section 3.4:

Theorem 1.2. *For any knot K , we have*

$$\begin{aligned} \max \{ \sigma(K) - 2v(K), 0 \} &\leq \hat{\gamma}_4^+(K), \\ \max \{ 2v(K) - \sigma(K), 0 \} &\leq \hat{\gamma}_4^-(K). \end{aligned}$$

1.3. Alternating Knots and the Turaev Genus. Setting aside connections to 4-dimensional bounds for the moment, we next shift to dimension 3 to completely characterize when the positive and negative Euler-normalized non-orientable 3-genera both vanish.

Theorem 1.3. *A knot K is alternating if and only if $\hat{\gamma}_3^+(K) = 0 = \hat{\gamma}_3^-(K)$.*

This theorem shows that the Euler-normalized non-orientable 3-genus can be thought of as a measurement of distance of a knot to the set of alternating knots. We make a connection between the stable non-orientable 3-genus and another such measurement, the Turaev genus. The Turaev genus g_T was developed by Turaev to study the Jones polynomial and the Tait conjectures, and was formalized in [12]; see Section 4.2 for the relevant definitions. As in Theorem 1.3, the Turaev genus of K vanishes if and only if K is alternating. We obtain the following bound.

Theorem 1.4. *For any knot K , $\bar{\gamma}_3(K) \leq g_T(K)$.*

As a corollary, we obtain a new family of torus knots with arbitrarily high Turaev genus.

Corollary 1.5. *For $k \geq 1$, $g_T(T(2k, 2k-1)) \geq k-1$.*

In fact, since the Turaev genus is realized on an adequate diagram [31], we make the following conjecture, which holds for knots of Turaev genus at most 1.

Conjecture 1.6. *For an adequate knot K , $g_T(K) = \bar{\gamma}_3(K)$.*

The proof of Theorem 1.3 also suggests a connection to the Jones polynomial and the Slope Conjecture. The proof of the forward direction of Theorem 1.3 is reminiscent of Curtis and Taylor’s proof that the largest (resp. smallest) boundary slope of a basic state surface of an alternating knot K is equal to the signature plus twice the maximum (resp. minimum) degree of the Jones polynomial [10]. The surfaces that realize $\hat{\gamma}_3^\pm(K)$ for an alternating knot K are precisely those that realized Curtis and Taylor’s Jones polynomial bound. This points to a potential connection between $\hat{\gamma}_3^\pm$ and the Slope Conjecture [16], at least for alternating, and perhaps even adequate, knots.

1.4. Genus Gaps. Building upon the notion of a slice knot, it is interesting to compare the 3- and 4-genera of a knot. We first address the classical question of how large the gap between $\gamma_3(K)$ and $\gamma_4(K)$ can be. Jabuka and Van Cott proved that $\gamma_3(K) - \gamma_4(K)$ may be arbitrarily large for families of torus knots [29]. We show that the gap is also arbitrarily large for a family of pretzel knots.

Proposition 1.7. *For any $n \geq 1$ and positive odd integers $k, r, p_1, \dots, p_{n-1}$, the pretzel knot $P = P(-k, r, -r - 1, p_1, -p_1, \dots, p_{n-1}, -p_{n-1})$ satisfies*

- (1) $\gamma_4(P) = 1$,
- (2) $\gamma_3(P) = 2n$, and
- (3) $g_4(P) \geq \frac{1}{2}(k - r - 2)$.

The gap between the Euler-normalized genera $\hat{\gamma}_3^\pm(P)$ and $\hat{\gamma}_4^\pm(P)$, on the other hand, is at most 2, though it is unclear if it is exactly 2. To find a non-trivial gap between Euler-normalized genera, we instead examine pretzel knots of the form $P_n = P(-3, 3, n)$ for odd $n \geq 3$. Knots of this form are slice [20]. Hence, we obtain $\hat{\gamma}_4^\pm(P_n) = 0$. In contrast, the negative Euler-normalized non-orientable 3-genus of P_n is non-vanishing.

Proposition 1.8. *For all odd $n \geq 3$, we have $\hat{\gamma}_3^-(P(-3, 3, n)) = 2$, while $\hat{\gamma}_3^+(P(-3, 3, n)) = 0$.*

Though the result in Proposition 1.8 could have been derived from Theorem 1.3, Theorem 1.4, and the fact that non-alternating pretzel knots have Turaev genus 1 [2], the ideas underlying the calculation, which include enumerating essential surfaces in the exterior of P_n , demonstrate what may be needed to prove Conjecture 1.6.

We end by showing that the gap between the Euler-normalized non-orientable 3- and 4-genera may be arbitrarily large. Specifically, we show that the Euler-normalized non-orientable 3-genus is additive under connected sum (see Lemma 7.1) and use that fact to prove:

Theorem 1.9. *For all $n \in \mathbb{N}$, there exists a knot K_n such that*

$$\hat{\gamma}_3^-(K_n) - \hat{\gamma}_4^-(K_n) = 2n.$$

Note that the same result for $\hat{\gamma}^+$ holds by taking mirror images.

1.5. Plan of the Paper. The remainder of the paper is organized as follows: we review non-orientable spanning surfaces and their geography in Section 2. A parallel discussion of non-orientable fillings and their geography appears in Section 3, culminating in a proof of Theorem 1.2. In Section 4, we explore alternating knots (including a proof of Theorem 1.3) and the Turaev genus (including a proof of Theorem 1.4). Next, we examine situations in which $\gamma_3(K) > \gamma_4(K)$ (Section 5, which includes a proof of Proposition 1.7) and where $\hat{\gamma}_3^\pm(K) > \hat{\gamma}_4^\pm(K)$ (Section 6, which includes a proof of Proposition 1.8). We end in Section 7 with a discussion of the behavior of $\hat{\gamma}_3^\pm$ under connected sum, which yields a proof of Theorem 1.9.

Acknowledgements. We thank David Futer for a series of enlightening discussions about the context and potential implications of this work. We further thank the participants of the Philadelphia Area Contact / Topology (PACT) Seminar for their feedback on a presentation of work in progress.

2. SPANNING SURFACES IN 3 DIMENSIONS

The goal of this section is to describe the framework necessary to investigate the non-orientable spanning surfaces of a knot. We start by reviewing the boundary slope of a spanning surface and by adapting Allen's geography problem to the 3-dimensional setting; this material appears in Section 2.1. In Sections 2.2 and 2.3, we present two well-known constructions of spanning surfaces. We finish with a discussion of essential surfaces, their boundary slopes, and their relationship to the 3-dimensional geography of a knot in Section 2.4.

2.1. Boundary Slope and 3-Dimensional Geography. A possibly non-orientable spanning surface F of a knot $K \subset S^3$ has two natural homological invariants: its **first Betti number** $b_1(F)$ and its **boundary slope** $s(F)$. To define the boundary slope, we push K a small amount along F to obtain a knot K' ; the boundary slope is then given by

$$s(F) = \text{lk}(K, K').$$

For later comparison with fillings in four dimensions, we also define the **(3-dimensional) normal Euler number** of F to be $e_3(F) = -s(F)$. See Figure 3 for an example of a trefoil knot bounding a Möbius strip F with $e_3(F) = -6$.

The boundary slope has several useful properties. First, the boundary slope vanishes on orientable surfaces. Second, the boundary slope is always even [2, Proposition 2.2]. In fact, the proof of Proposition 2.2 in [2] shows that

$$(2.1) \quad e_3(F) \equiv s(F) \equiv 2b_1(F) \pmod{4}.$$

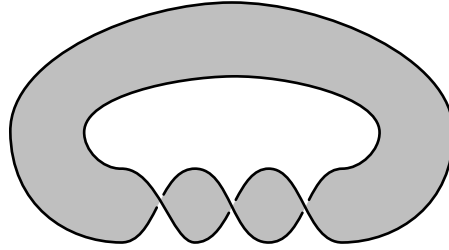


FIGURE 3. A trefoil knot K bounding a Möbius strip F with $e_3(F) = -6$. Each crossing of K induces four crossings (all positive) between K and the pushoff K' .

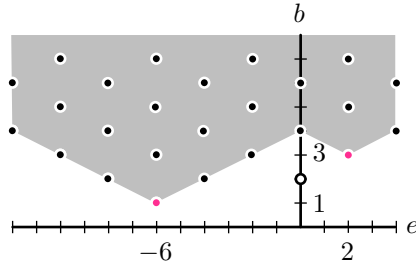


FIGURE 4. The three-dimensional geography $R_3(K)$ for the trefoil knot K , with each solid dot denoting a point realized by a spanning surface. The vertex at $(-6, 1)$ is the Möbius strip in Figure 3, while the vertex $(2, 3)$ is the positive twist of the Seifert surface. The Seifert surface itself is denoted by an open dot at $(0, 2)$.

We organize our exploration of spanning surfaces of a knot K by adapting Allen's geography question for fillings in 4 dimensions to the 3-dimensional setting.

Definition 2.1 (Adapted from [3]). The **three-dimensional geography of a knot** K is the subset $R_3(K) \subset 2\mathbb{Z} \times \mathbb{N}$ of all pairs $(e_3(F), b_1(F))$ for $F \in \mathcal{F}_3(K)$. An element $(e, b) \in R_3(K)$ is called **realizable**.

We typically depict the geography of a knot on a $2\mathbb{Z} \times \mathbb{N}$ grid. For example, Figure 4 shows the 3-dimensional geography of the trefoil knot. We will verify the correctness of the figure in the next section.

The addition of a twisted band is an important operation in the study of the 3-dimensional geography. Note once again that we define the sign of a twisted band in terms of the normal Euler number, not the boundary slope. The twisted band operation motivates the definition of a **wedge** $W_{(E,B)} \subset 2\mathbb{Z} \times \mathbb{N}$, which consists of pairs (e, b) that satisfy Equation (2.1)

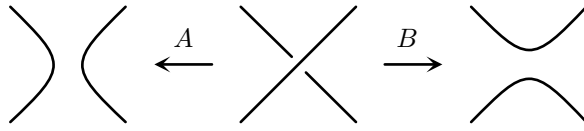


FIGURE 5. A crossing of a knot diagram can be split with an A -resolution or a B -resolution.

and the relation

$$\frac{1}{2}|e - E| \leq b - B.$$

If F is a spanning surface, we write W_F for $W_{(e_3(F), b_1(F))}$. The addition of twisted bands shows that if F is a spanning surface for K , then $W_F \subset R_3(K)$. In fact, we have

$$(2.2) \quad R_3(K) = \bigcup_{F \in \mathcal{F}_3(K)} W_F.$$

2.2. Construction: State Surfaces. The state surface construction generalizes both the Seifert algorithm and checkerboard surfaces; see [2] or [32], for example. To set notation, we recall the definition of a state of a knot diagram. First, we define a **resolution** for a crossing of an unoriented link diagram D to be a choice of splitting the crossing into two separate segments in one of two possible ways: an A -resolution or a B -resolution, as shown in Figure 5. A **state** s of a knot diagram D is the configuration of disjoint, possibly nested, simple closed curves (called **state circles**) in the plane that is produced by applying either an A - or B -resolution at every crossing of D . Let $A(s)$ (resp. $B(s)$) be the number of A resolutions (resp. B resolutions) in the state s .

To associate a surface to a state s , fill each state circle with a disk, thinking of disks of inner nested state circles as lying above those of outer nested state circles in \mathbb{R}^3 . Connect the disks with half-twisted bands where the crossings were. We say that a state surface is **basic** if no bands connect a state circle to itself. Examples of basic state surfaces for the 5_2 knot are given below in Figure 6.

State surfaces play a particularly important role for the 3-dimensional geography of alternating knots due to the following result of Adams and Kindred.

Theorem 2.2 (Theorem 5.4 of [2]). *Given a diagram D and a spanning surface F of a knot K , there exists a basic state surface F_s of the same orientability as F and a (possibly empty) set of twisted bands transforming F_s into F'_s so that $b_1(F'_s) = b_1(F)$ and $e_3(F'_s) = e_3(F)$.*

This theorem essentially says that state surfaces generate the 3-dimensional geography of a knot. In particular, we can refine Equation (2.2) for alternating knots as follows.

Corollary 2.3. *Given a diagram D of a knot K , let \mathcal{S}_n be the set of non-orientable basic state surfaces for D , let $\text{tw}_\pm(\mathcal{S}_o)$ be the set of orientable basic state surfaces with one \pm -twisted band attached, and finally let $\mathcal{S} = \mathcal{S}_n \cup \text{tw}_+(\mathcal{S}_o) \cup \text{tw}_-(\mathcal{S}_o)$. Then*

$$R_3(K) = \bigcup_{F \in \mathcal{S}} W_F.$$

The normal Euler number of a state surface may be computed combinatorially. We denote by $\text{wr}(D)$ the writhe of a knot diagram D .

Lemma 2.4 (Proposition 3.2 of [2]). *If F_s is a state surface arising from a state s of a diagram D , then¹*

$$e_3(F_s) = A(s) - B(s) - \text{wr}(D).$$

Example 2.5. Of the eight state surfaces for the diagram of the trefoil in Figure 3, exactly two are basic. These basic state surfaces arise from the all- A state s_A , which yields the Seifert surface, and the all- B state s_B , which yields the Möbius strip in Figure 3. By Lemma 2.4, we compute

$$\begin{array}{ll} e_3(F_{s_A}) = 0 & e_3(F_{s_B}) = -6 \\ b_1(F_{s_A}) = 2 & b_1(F_{s_B}) = 1. \end{array}$$

Corollary 2.3 implies that the geography of the trefoil is generated by wedges based at $(-6, 1)$ (from F_{s_B}), $(-2, 3)$, and $(2, 3)$ (from adding twists to the Seifert surface F_{s_A}). This justifies the geography depicted in Figure 4.

Example 2.6. Of the 32 state surfaces for the diagram of the 5_2 knot in Figure 6, only three are basic: the all- A state surface F_{s_A} , the all- B state surface F_{s_B} , and one more state surface F_s ; see Figure 6.

As above, we compute that

$$\begin{array}{lll} e_3(F_{s_A}) = 10 & e_3(F_s) = 4 & e_3(F_{s_B}) = 0 \\ b_1(F_{s_A}) = 3 & b_1(F_s) = 2 & b_1(F_{s_B}) = 2. \end{array}$$

The all- B state surface is orientable, and hence Corollary 2.3 implies that the geography of the 5_2 knot is generated by wedges based at $(10, 3)$, $(4, 2)$, $(2, 3)$, and $(-2, 3)$. See Figure 7.

¹There is a sign error in [2, Proposition 3.2], which is corrected in the statement of Lemma 2.4.

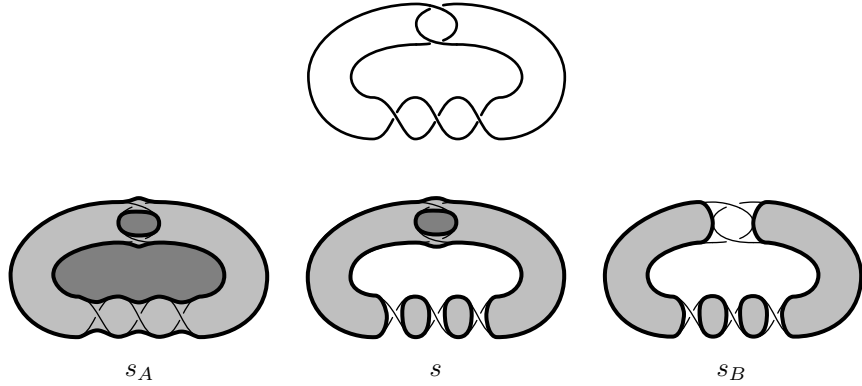


FIGURE 6. The three basic state surfaces for the diagram of the 5_2 knot at top.

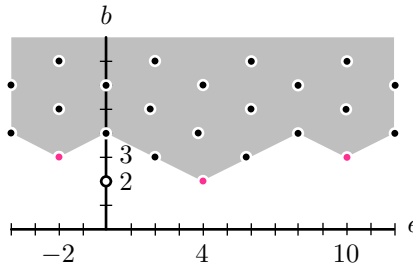


FIGURE 7. The 3-dimensional geography of the 5_2 knot is generated by the state surfaces for s_A at $(10, 3)$ and s at $(4, 2)$, along with the state surface s_B (which is depicted by an open dot at $(0, 2)$) with a negative twisted band at $(-2, 3)$.

2.3. Construction: Pinch Surfaces for Torus Knots. In this section, we describe the construction of a **pinch surface** of a torus knot $T(p, q)$ in the case that pq is even. This construction is due to Batson [5] for surfaces in B^4 and adapted to produce surfaces in S^3 in [29]; we follow the latter source here.

Working abstractly at first, realize $T(p, q)$ as a straight line on a flat torus as in Figure 8(a). Perform a (non-orientable) band move on $T(p, q)$ along a band that connects two adjacent strands, as in Figure 8(b), yielding a new torus knot $T(r, s)$. The parameters r, s satisfy [5, 30]

$$(2.3) \quad r = |p - 2t| \quad s = |q - 2h|$$

where $t \equiv -q^{-1} \pmod{p}$ and $h \equiv p^{-1} \pmod{q}$.

More concretely, place $T(p, q)$ on a standard torus in \mathbb{R}^3 so that it wraps p times around the longitude and q times around the meridian. Place $T(r, s)$ on a torus contained in the interior of the first. The band move above creates an embedded cobordism between the two knots.

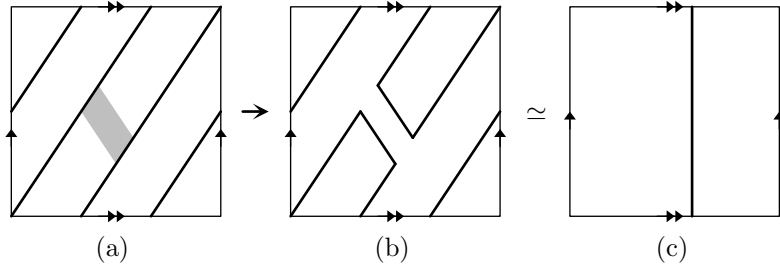


FIGURE 8. (a) A non-orientable band for $T(p, q)$, (b) performing a band move, and (c) isotoping the resulting knot to obtain $T(r, s)$.

Since the parity of pq is preserved by pinch moves [29, Lemma 2.1], repeated pinching of $T(p, q)$ yields the unknot $T(k, 1)$ with k even. Further pinch moves reduce k by 2, eventually yielding the meridian $T(0, 1)$. Capping the meridian by a disk finishes the construction of the 3-dimensional pinch surface $F_3(p, q)$.

As pointed out in [29], the pinch surface realizes the non-orientable 3-genus of $T(p, q)$, which was computed by Teregaito [42]. The first Betti number of $F_3(p, q)$ is given by the number of pinches. Further, we may compute the normal Euler number of the pinch surface.

Lemma 2.7 (Lemma 2.3 of [39] or Proposition 6 of [42]). *The pinch surface $F_3(p, q)$ has normal Euler number $e_3(F_3(p, q)) = -pq$.*

Example 2.8. The pinch surface for the trefoil knot $T(3, 2)$ coincides with the Möbius band in Figure 3. The result of Lemma 2.7, namely that $e_3(F_3(3, 2)) = -6$, agrees with the computations in Sections 2.1 and 2.2.

Remark 2.9. There is an extension of the pinch surface construction to the case where pq is odd that involves splitting $T(p, q)$ into a pair of even torus knots on the boundaries of complementary solid tori, and then applying the algorithm above to each of the resulting knots; see [29] for details.

2.4. Essential Surfaces. While the geography of alternating knots can be analyzed using state surfaces, not every class of knots has such a known “generating set”. In order to understand these classes, we must consider the set of incompressible and ∂ -incompressible surfaces in the complement of K .

We briefly recall some definitions of the required tools. Suppose Y is a 3-manifold with boundary and F is a properly embedded surface in Y . Below, we will only consider when Y is the exterior of a knot K , i.e. when Y is $E(K) = S^3 \setminus \nu(K)$. Choosing a meridian μ and Seifert-framed longitude λ for $\partial\nu(K)$, we write $[\partial F] = a[\mu] + b[\lambda]$. The **boundary slope** $s(F)$ is $\frac{a}{b} \in \mathbb{Q} \cup \{\frac{1}{0}\}$. This agrees with the definition of boundary slope for spanning surfaces, as for a spanning surface, $b = 1$ and a measures the linking number

with respect to the Seifert framing. As before, the **normal Euler number** $e_3(F)$ is the negation of the boundary slope. We extend Γ^\pm to any surface properly embedded in the exterior of a knot.

We follow [24] in defining a **compressing disk** for F to be an embedded disk $D \subset Y$ with $D \cap F = \partial D$. The surface F is **incompressible** if for each compressing disk D , there is a disk $D' \subset F$ with $\partial D' = \partial D$. Similarly, a **∂ -compressing disk** of F is an embedded disk $D \subset Y$ with $D \cap F = \alpha$ and $D \cap \partial Y = \beta$, where $\alpha \cup \beta = \partial D$ and $\alpha \cap \beta = S^0$. The surface F is **∂ -incompressible** if for each ∂ -compressing disk D , there is a disk $D' \subset F$ with $\partial D' = \alpha \cup \beta'$ with $\beta' \subset \partial F$. A **compression** along a compressing or ∂ -compressing disk is a surgery along the compressing or ∂ -compressing disk. Finally, we say that a surface that is incompressible and ∂ -incompressible, or is a sphere not bounding a ball, or is a disk that is not ∂ -parallel, is **essential**.

To understand how essential surfaces are related to the 3-dimensional geography of a knot K , we define, for any $(u, v) \in \mathbb{Q} \times \mathbb{N}$, the **rational wedge based at (u, v)** by

$$\tilde{W}_{(u,v)} = \{(e, b) \in \mathbb{Q} \times \mathbb{N} : |e - u| \leq 2(b - v)\}.$$

If F is a properly embedded surface in $E(K)$, we set the notation $\tilde{W}_F = \tilde{W}_{(e_3(F), b_1(F))}$. Now let $\mathcal{F}(K)$ denote the set of all incompressible and ∂ -incompressible surfaces in $E(K)$, which is a finite set by [22]. Define the **incompressible wedge** of K to be

$$\tilde{W}(K) = \bigcup_{F \in \mathcal{F}(K)} \tilde{W}_F.$$

We may now state the main structural result in this section, which constrains the non-orientable 3-dimensional geography of a knot K using knowledge of the incompressible and ∂ -incompressible surfaces in its exterior. This should be thought of as an analogue of Corollary 2.3.

Proposition 2.10. *For each knot K , $R_3(K) \subset \tilde{W}(K)$.*

The key technical idea in the proof is that we can bound the change in boundary slopes under a ∂ -compression.

Lemma 2.11. *Given a knot K and a properly embedded surface $F \subset E(K)$, let F' be the result of a ∂ -compression of F . The difference between the boundary slopes (and hence the normal Euler number) is bounded by 2, i.e.*

$$|e_3(F') - e_3(F)| \leq 2.$$

If F is incompressible, then we get equality in the bound above if and only if both F and F' are spanning surfaces.

Proof. We first suppose that F has boundary slope 0, i.e. ∂F is a canonical longitude λ of the boundary torus T . Recall that a ∂ -compressing disk D imprints an embedded arc β on T that intersects ∂F precisely at its endpoints.

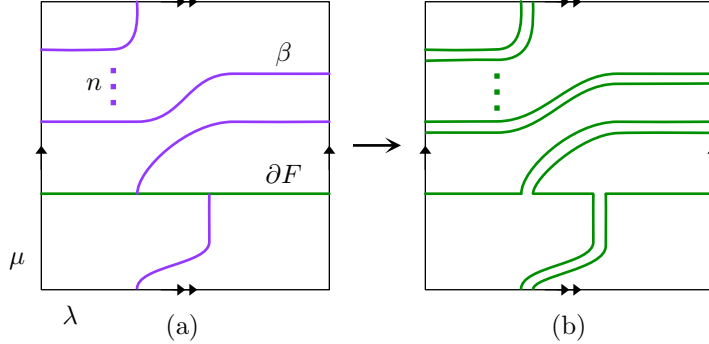


FIGURE 9. (a) The curve β when it intersects ∂F on two sides. (b) The result at the boundary of a ∂ -compression along D .

Arguing as in the proof of Theorem 1 of [25], we see that β either intersects ∂F on one or two sides in T . If β intersects ∂F on one side, then β and a subarc of ∂F bound a disk in T . That disk, when pushed slightly into $E(K)$, combines with the ∂ -compressing disk D to yield a compressing disk D' . Thus, ∂ -compression along D is tantamount to compression along D' , and hence F and F' have the same boundary slope.

If, on the other hand, β intersects F on two sides, then up to isotopy, β must be of the form pictured in Figure 9(a) for some $n \in \mathbb{Z}$. That is, after adding a subarc of ∂F to obtain a closed curve $\hat{\beta}$, we must have that $[\hat{\beta}]$ is of the form $n\mu + \lambda$. Performing a ∂ -compression along D yields $2n$ additional longitudes and 2 additional meridians for $\partial F'$; see Figure 9(b). In particular, we have $[\partial F'] = 2\mu + (2n + 1)\lambda$.

More generally, suppose that F has boundary slope $\frac{p}{q}$. Consider the automorphism ϕ of T represented by the matrix

$$\begin{bmatrix} r & p \\ s & q \end{bmatrix} \in SL(2, \mathbb{Z}).$$

In particular, we may assume that $rq - ps = 1$ and $0 \leq s < q$. The automorphism ϕ carries the longitude λ to ∂F . By the first case, we know that $\phi^{-1}(\partial F') = 2\mu + (2n + 1)\lambda$ for some $n \in \mathbb{Z}$. Thus, the boundary slope of F' may be written as

$$s(F') = \frac{2r + (2n + 1)p}{2s + (2n + 1)q}.$$

We then use the fact that $\phi \in SL(2, \mathbb{Z})$ to compute that

$$(2.4) \quad |s(F') - s(F)| = \left| \frac{2}{q(2s + (2n + 1)q)} \right| \leq 2,$$

which proves the bound stated in the lemma.

To prove the last statement of the lemma, first note that the incompressibility of F implies, as above, that β intersects ∂F on two sides in $\partial E(K)$. Next, if we have equality in Equation (2.4), then $q = 1$. When $q = 1$, since $0 \leq s < q$, we see that s must be 0, and hence so must n . Thus, we see that F and F' are both spanning surfaces. Conversely, if F is a spanning surface, then $q = 1$ (and hence $s = 0$), and if F' is a spanning surface, then $1 = 2s + (2n + 1)q = 2n + 1$, and hence $n = 0$, which yields equality in Equation (2.4). \square

Proof of Proposition 2.10. Suppose that $(e, b) \in R_3(K)$, i.e. that there is a spanning surface F for K with $e_3(F) = e$ and $b_1(F) = b$. By a sequence of compressions and ∂ -compressions

$$F = F_0 \rightarrow F_1 \rightarrow \cdots \rightarrow F_n = F',$$

we arrive at an imcompressible and ∂ -incompressible surface F' properly embedded in the exterior $E(K)$.

We claim that $(e, b) \in \tilde{W}_{F'}$; the proposition will then follow. In fact, it suffices to show that the line segment ℓ_i joining $(e_3(F_i), b(F_i))$ to $(e_3(F_{i+1}), b(F_{i+1}))$ has slope at least $\frac{1}{2}$ in absolute value. If F_{i+1} is obtained from F_i by a compression, then the boundary slopes of F_i and F_{i+1} agree, so the line segment ℓ_i has infinite slope. If F_{i+1} is obtained from F_i by a ∂ -compression, then $b_1(F_i) - b_1(F_{i+1}) = 1$ and Lemma 2.11 shows that $|e_3(F_i) - e_3(F_{i+1})| \leq 2$. Thus, we have that the slope of ℓ_i is at least $\frac{1}{2}$ in absolute value. \square

As a corollary of the proof, we obtain a bound on the values of Γ^\pm of surfaces properly embedded in the exterior of K .

Corollary 2.12. *Given a knot K and a properly embedded $F \subset E(K)$, we have*

$$\Gamma^\pm(F) \geq \min\{\Gamma^\pm(F') : F' \in \mathcal{F}(K)\}.$$

3. FILLINGS IN 4 DIMENSIONS

Our next step is to describe the framework necessary to investigate the non-orientable 4-genus of a knot. In parallel to the 3-dimensional setting, we first review the normal Euler number and Allen's geography problem in Section 3.1. Next, in Section 3.2, we revisit pinch surfaces in 4 dimensions. We finish the section by describing lower bounds on the non-orientable 4-genus in Sections 3.3 and 3.4, including a proof of Theorem 1.2.

3.1. Normal Euler Number and 4-Dimensional Geography. As in the 3-dimensional setting, non-orientable fillings carry a second homological invariant: the normal Euler number, which captures the topology of the normal bundle. We present two equivalent definitions of the normal Euler number of a **cobordism** between two links. A cobordism is a properly embedded, compact surface $F \subset [0, 1] \times S^3$ with boundary $\partial F = K_0 \cup K_1$ such that $K_i \subset \{i\} \times S^3$. A filling for a knot K is a cobordism with $K_1 = K$ and $K_0 = \emptyset$.

First, following [19], let F' be the result of pushing F along a nonzero section of its normal bundle. Let $\partial F' = K'_0 \sqcup K'_1$, and define the **normal Euler number** of F by

$$(3.1) \quad e_4(F) = \text{lk}(K_0, K'_0) - \text{lk}(K_1, K'_1).$$

In the case where the cobordism F arises from attaching a flat band to a diagram D_0 to obtain D_1 , the normal Euler number may be computed using the blackboard framing in the formula in [38, Lemma 4.2]:

$$(3.2) \quad e_4(F) = \text{wr}(D_0) - \text{wr}(D_1).$$

Second, following [38], let F'' be a small transverse push-off of F so that the pushoffs at the ends K''_i both realize the Seifert framings of K_i . The normal Euler number $e_4(F)$ may be computed by choosing compatible local orientations of $T_x F$ and of $T_x F''$ at each point $x \in F \cap F''$, then comparing the resulting orientation on $T_x F \oplus T_x F''$ to the ambient orientation on $[0, 1] \times S^3$, and finally adding up these local contributions.

It is straightforward to check using Equation (3.1) that the normal Euler number of a spanning surface F that has been pushed into B^4 agrees, up to a sign, with normal Euler number of F defined in Section 2.1. More precisely, we have:

Lemma 3.1. *If F is a spanning surface of a knot K , and F' is the result of pushing F into B^4 relative to K , then*

$$e_4(F') = e_3(F) = -s(F).$$

As a result of this lemma, we no longer distinguish between the 3- and 4-dimensional normal Euler numbers of a surface F , denoting both by $e(F)$.

The normal Euler number satisfies several useful properties: it is always even, it vanishes on orientable surfaces, it is additive under concatenation of cobordisms, and, as shown in [36], it satisfies

$$(3.3) \quad e(F) \equiv 2b_1(F) \pmod{4}.$$

Definition 3.2 ([3]). The **four-dimensional geography** of a knot K is the subset $R_4(K) \subset 2\mathbb{Z} \times \mathbb{N}$ of all pairs $(e(F), b_1(F))$ for $F \in \mathcal{F}_4(K)$.

We may translate the addition of a twisted band from the 3- to the 4-dimensional setting. The definition of a wedge for the four-dimensional geography is equivalent to that presented in Section 2.1.

Example 3.3. That the three- and four-dimensional geographies of the trefoil are identical follows from our work from Section 2 and Proposition 3.1 in [3]. The 5_2 knot, however, provides an example where the 3-dimensional geography is a strict subset of the 4-dimensional geography. In Figure 10, we display a filling F of the 5_2 knot arising from a flat band move. Using Equation (3.2), we compute that $e(F) = 2$ and $b_1(F) = 1$. Recalling Example 2.6, we see that the point $(2, 1) \in R_4(K)$, but $(2, 1) \notin R_3(K)$.

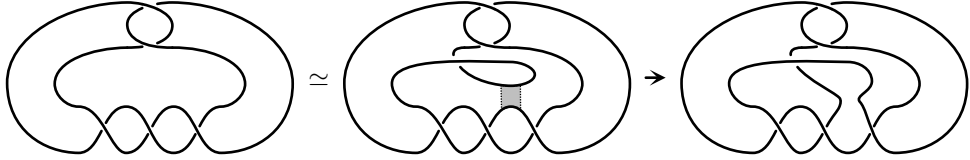


FIGURE 10. A Möbius strip filling of the 5_2 knot with normal Euler number 2 arises from an isotopy, an attachment of a flat band, and finally an isotopy to the unknot.

3.2. Construction: Pinch Surfaces, Revisited. The pinch surface construction for torus knots described in Section 2.3 extends to finding fillings in B^4 — in fact, that was the design of the original description in [5]. For any positive, relatively prime (p, q) , use the pinch move to create a non-orientable cobordism in successive layers of B^4 from $T(p, q)$ down to the first instance of $T(r, 1)$. Since $T(r, 1)$ is an unknot, we can cap it off with a disk in B^4 , yielding a filling surface $F_4(p, q)$.

Lemma 3.4 (Lemma 2.3 of [39]). *If $T(p, q)$ is transformed into $T(r, 1)$ in the construction of $F_4(p, q)$, then*

$$e(F(p, q)) = r - pq.$$

3.3. Signature and the Gordon-Litherland Bound. To complement the constructions of non-orientable spanning surfaces and fillings discussed thus far, we now turn to lower bounds. We begin by recalling Gordon and Litherland’s symmetric bilinear pairing $\langle \cdot, \cdot \rangle_F$ on the first homology of a compact embedded surface $F \subset S^3$. The unit normal bundle $\nu_1(F)$ is a 2-fold cover $p : \nu_1(F) \rightarrow F$ and embeds into $S^3 \setminus F$. For a pair of classes $a, b \in H_1(F)$ represented by embedded, oriented multicurves $\alpha, \beta \subset F$, define

$$\langle a, b \rangle_F = \text{lk}(\alpha, p^{-1}\beta).$$

This is a well-defined symmetric bilinear pairing [19], and we write $\sigma(F)$ for its signature. The signature of the pairing $\langle \cdot, \cdot \rangle_F$ is related to the signature of K and the normal Euler number of F .

Proposition 3.5 (Corollary 5 of [19]). *If F is a spanning surface of a knot K , then*

$$\sigma(K) = \sigma(F) + \frac{e(F)}{2}.$$

As a corollary, we obtain what is commonly termed the Gordon-Litherland inequality; see Corollary 2.5 of [3].

Theorem 3.6. *Let $K \subset S^3$ be a knot and let F be a filling of K . Then*

$$\left| \sigma(K) - \frac{e(F)}{2} \right| \leq b_1(F).$$

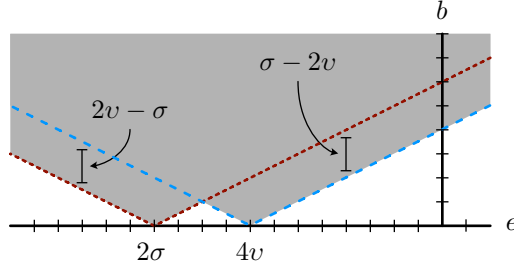


FIGURE 11. The wedges $W_\sigma(K)$ and $W_v(K)$ restrict the 4-dimensional (and hence 3-dimensional) non-orientable geography of a knot K . The bound in Corollary 3.8 is the height of the vertex of $W_\sigma(K) \cap W_v(K)$, while the vertical distances between the edges of the wedges yield the bounds in Theorem 1.2. The values for σ and v are taken from $T(4, 3)$.

Reinterpreting this inequality in terms of the Euler-normalized first Betti number, we obtain, for any filling F , the inequality

$$\Gamma_4^\pm(F) \geq 0,$$

hence justifying taking the minimum in the definition of the Euler-normalized non-orientable genus.

The Gordon-Litherland inequality restricts the 3- and 4-dimensional geography of a knot K to lie in the wedge $W_\sigma(K)$ based at $(2\sigma(K), 0)$; see Figure 11. As noted in the introduction, the Euler-normalized non-orientable genera measure the minimum vertical distance from $R_*(K)$ to the boundary of $W_\sigma(K)$.

3.4. Further Bounds. The Gordon-Litherland inequality is not the only bound on $b_1(F)$ and $e(F)$. In fact, there is a class of what Sato [40] calls “non-orientable slice-torus invariants” that yield structurally similar bounds. Of importance in this paper is the v invariant derived from Heegaard-Floer homology.

Theorem 3.7 (Theorem 1.1 of [38]). *For any filling F of a knot K , we have*

$$\left| 2v(K) - \frac{e(F)}{2} \right| \leq b_1(F).$$

As with the Gordon-Litherland inequality, Theorem 3.7 restricts the possible pairs (e, b) for surfaces in B^4 spanning a given knot K to a wedge $W_v(K)$ based at $(4v(K), 0)$; see Figure 11 again.

The standard next step is to combine Theorems 3.6 and 3.7 to obtain a lower bound on the non-orientable 4-genus.

Corollary 3.8 (Theorem 1.2 of [38]). *For any knot K , we have*

$$\left| v(K) - \frac{\sigma(K)}{2} \right| \leq \gamma_4(K).$$

We are now ready to prove Theorem 1.2. The bound in Corollary 3.8 can be visualized as the height of the base of the wedge $W_\sigma(K) \cap W_v(K)$; see Figure 11 once again. Inspired by this visualization, we may also extract a lower bound on the Euler-normalized non-orientable 4-genus, as the quantity $|2v(K) - \sigma(K)|$ measures the vertical distance between the boundaries of $W_\sigma(K)$ and $W_v(K)$. Theorem 1.2 follows.

4. EULER-NORMALIZED GENUS AGREEMENTS: ALTERNATING KNOTS AND THE TURAEV GENUS

We return to dimension 3 to examine the Euler-normalized non-orientable genera of alternating knots (Section 4.1), which leads to a connection to the Turaev genus (Section 4.2). We also explore some examples of torus knots in Section 4.3, and call attention to the relationship between the 3- and 4-dimensional Euler-normalized non-orientable genera for the knots examined in this section.

4.1. Alternating Knots. The goal of this section is to prove Theorem 1.3, i.e. that a knot is alternating if and only if both of its stable non-orientable 3-genera vanish. We first prove the forward implication using a combinatorial approach, and then prove both implications using a topological approach based on Greene's characterization of alternating knots. We note that the ideas in the combinatorial approach closely match those in [10], where the genera of non-orientable spanning surfaces for alternating knots were related to degrees of the Jones polynomial.

4.1.1. Combinatorial Proof of Theorem 1.3. Let F_A (resp. F_B) be the all- A (resp. all- B) state surface of a reduced alternating diagram D of K . It suffices to show that $\Gamma^+(F_A) = 0 = \Gamma^-(F_B)$. In particular, we will show that

$$(4.1) \quad b_1(F_A) = \frac{e(F_A)}{2} - \sigma(K).$$

A similar proof works for F_B .

First, we set notation. The number of crossings of a diagram D is denoted cr , with cr_+ (resp. cr_-) the number of positive (resp. negative) crossings. For a state s , let $|s|$ denote the number of state circles. For the standard checkerboard shading of a reduced alternating diagram D , the state circles of s_A (resp. of s_B) correspond to the white (resp. black) regions.

There are three main inputs into the proof. The first is a computation of the normal Euler and Betti numbers of the state surfaces F_A and F_B .

Lemma 4.1. *For a diagram D of a knot K ,*

$$\begin{aligned} e(F_A) &= 2cr_- & e(F_B) &= -2cr_+ \\ b_1(F_A) &= 1 - |s_A| + cr & b_1(F_B) &= 1 - |s_B| + cr \end{aligned}$$

The proof follows from Lemma 2.4 and the construction of the state surfaces. Alternatively, the computations of the normal Euler numbers appear as Lemma 5 in [15].

The second input is a fact about the combinatorics of an alternating diagram.

Lemma 4.2. *A diagram D of an alternating knot K satisfies*

$$2 = -\text{cr} + |s_A| + |s_B|.$$

The proof follows from $\chi(S^2) = 2$, the fact that a reduced alternating diagram yields a cell decomposition of S^2 , and the observation that an A -split separates adjacent white regions.

The last input computes the signature of an alternating knot directly from its diagram.

Lemma 4.3 (Theorem 2 of [43]). *Given an alternating knot K with reduced alternating diagram D , we have*

$$\sigma(K) = \frac{1}{2}(-\text{wr}(D) + |s_A| - |s_B|).$$

We are now ready to prove the relation in Equation (4.1), and hence the forward direction of Theorem 1.3. We compute as follows:

$$\begin{aligned} \frac{1}{2}e(F_A) - b_1(F_A) &= \text{cr}_- - 1 + |s_A| - \text{cr} && \text{(Lemma 4.1)} \\ &= -\text{cr}_+ + \frac{1}{2}(\text{cr} - |s_A| - |s_B|) + |s_A| && \text{(Lemma 4.2)} \\ &= -\sigma(K) && \text{(Lemma 4.3)} \end{aligned}$$

4.1.2. *Topological Proof of Theorem 1.3.* An alternative approach to the proof of Theorem 1.3 uses Greene's topological characterization of alternating links [21], adjusted slightly to our setting. We say that a spanning surface F is **positive** (resp. **negative**) **definite** if the Gordon-Litherland form $\langle \cdot, \cdot \rangle_F$ is positive (resp. negative) definite.

Theorem 4.4 ([21]). *A knot $K \subset S^3$ is alternating if and only if K bounds both a positive and a negative definite spanning surface.*

First, suppose K is an alternating knot. By Theorem 4.4, K bounds a positive definite surface F_+ . Combining the positive definiteness with Proposition 3.5, we see that

$$b_1(F_+) = \sigma(F_+) = \sigma(K) - \frac{e(F_+)}{2}.$$

It follows immediately that $\hat{\gamma}_3^+(K) = 0$. Similarly, since K also bounds a negative definite surface F_- , we have $\hat{\gamma}_3^-(K) = 0$.

Conversely, the calculations above show that if $\hat{\gamma}_3^\pm(K) = 0$, then K must bound both a positive and a negative definite surface. Hence, by Theorem 4.4, K must be alternating.

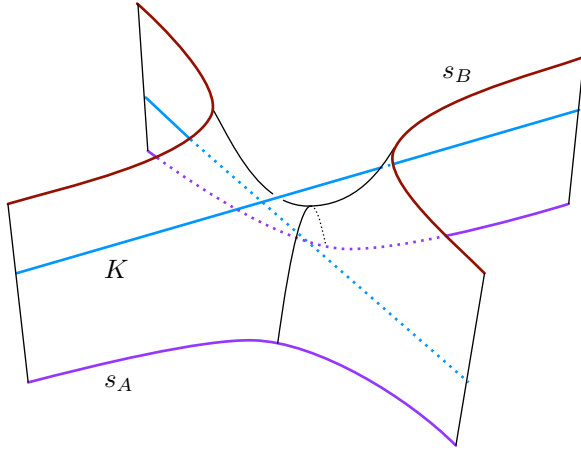


FIGURE 12. Connecting the state circles over the edges and near the crossings of a diagram D to create a cobordism between s_A and s_B .

4.2. Relation to the Turaev Genus. The Turaev genus g_T of a knot diagram D measures the difference between the all- A and the all- B state circles of the diagram. Specifically, we construct the Turaev surface F_T of D by taking a copy of the all- A state circles s_A just above the plane of the diagram D and a copy of the all- B state circles s_B just below D . Over the edges of D , connect the state circles with a rectangular strip; near the crossings of D , connect them with a saddle as in Figure 12. This creates a cobordism between s_A and s_B . Finally, cap off each of the state circles with a disk. The **Turaev genus of the diagram** D is the genus of the Turaev surface F_T , which may be computed as

$$(4.2) \quad g_T(D) = \frac{1}{2} (\text{cr} + 2 - |s_A| - |s_B|).$$

The **Turaev genus $g_T(K)$ of a knot K** is the minimum of the Turaev genera over all possible diagrams of K . See the original paper [12], the survey [8], or [31] for further discussion.

We are now ready for the proof of Theorem 1.4.

Proof of Theorem 1.4. It suffices to show that, for any diagram D of a knot K , we have

$$g_T(D) = \frac{1}{2} (\Gamma^+(F_A) + \Gamma^-(F_B)).$$

This relation follows directly from the definition of Γ^\pm , Lemma 4.1, and a short computation. \square

The bound in Theorem 1.4 is not always realized, as discussed in the next section. For an adequate knot, however, we conjecture that the bound is

sharp; this was the statement of Conjecture 1.6. Theorem 1.3 shows that the conjecture holds for all alternating knots, and Theorem 1.4 implies that the conjecture holds for all Turaev genus 1 knots. In order to prove the full conjecture, however, we would need to understand all possible spanning surfaces of adequate knots or, alternatively, all possible essential surfaces in the exterior of the knot. We will demonstrate how the latter type of argument would work in Section 6.

4.3. Torus Knots. Theorem 1.3 implies that the Euler-normalized non-orientable 3- and 4-dimensional non-orientable genera agree for alternating knots. The torus knot $T(4, 3)$ displays similar behavior, even though its ordinary 3- and 4-dimensional genera differ. Further, as with alternating knots, the bound in Theorem 1.4 for $T(4, 3)$ is sharp, though non-zero.

Proposition 4.5. *The torus knot $T(4, 3)$ has the following properties:*

- (1) $\gamma_3(T(4, 3)) > \gamma_4(T(4, 3))$,
- (2) $\hat{\gamma}_3^+(T(4, 3)) = 0 = \hat{\gamma}_4^+(T(4, 3))$ while $\hat{\gamma}_3^-(T(4, 3)) = 2 = \hat{\gamma}_4^-(T(4, 3))$,
and
- (3) $g_T(T(4, 3)) = 1 = \bar{\gamma}_3(T(4, 3))$.

Proof. The first part of the proposition follows from the computation that $\gamma_3(T(4, 3)) = 2$ and $\gamma_4(T(4, 3)) = 1$; see [29, Example 5.3] or the entry for $8_{19} = T(4, 3)$ in [34]. These values are realized using pinch surfaces, which have

$$\begin{aligned} e(F_3(4, 3)) &= -12 & e(F_4(4, 3)) &= -10 \\ b_1(F_3(4, 3)) &= 2 & b_1(F_4(4, 3)) &= 1. \end{aligned}$$

The proof of the second part starts with the computations $\sigma(T(4, 3)) = -6$ and $v(T(4, 3)) = -2$ using techniques from [30]. Thus, the bounds in Theorem 1.2 are sharp at the pinch surface $F_4(4, 3)$, and hence $\hat{\gamma}_4^+(T(4, 3)) = 0$ and $\hat{\gamma}_4^-(T(4, 3)) = 2$. The computations for the second part of the proof are summarized in terms of geography in Figure 13.

Turning to spanning surfaces of $T(4, 3)$ in S^3 , on the positive side, the minimal Seifert surface S has $e(S) = 0$ and $b_1(S) = 6$, and hence $\Gamma_3^+(\text{tw}_+(S)) = 0$. It follows that $\hat{\gamma}_3^+(T(4, 3)) = 0$. On the negative side, the pinch surface $F_3(4, 3)$ has first Betti number 2 and normal Euler number -12 , and hence has $\Gamma_3^-(F_3(4, 3)) = 2$. As the lower bounds in Theorem 1.2 also apply to $\hat{\gamma}_3^\pm$, it follows that $\hat{\gamma}_3^-(T(4, 3)) = 2$ as well. Once again, see Figure 13.

Finally, we read off the computation $g_T(T(4, 3)) = 1$ from [1] or [35], while the work above yields $\bar{\gamma}_3(T(4, 3)) = 1$. \square

The torus knot $T(4, 3)$ is the first non-trivial example in the family of torus knots $T(2k, 2k - 1)$. Batson [5] showed that this family has unbounded γ_4 , with $\gamma_4(T(2k, 2k - 1)) = k - 1$. Further, all elements in the family have $R_4 = W_\sigma \cap W_v$ [39], which yields

$$\hat{\gamma}_4^-(T(2k, 2k - 1)) = 0 \quad \text{and} \quad \hat{\gamma}_4^+(T(2k, 2k - 1)) = 2k - 2.$$

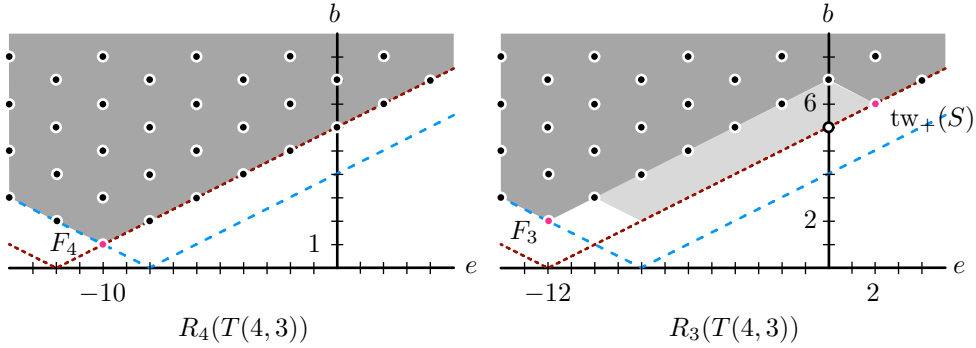


FIGURE 13. The 4-dimensional geography of the torus knot $T(4,3)$ is precisely $W_{F_4(p,q)}$, while the 3-dimensional geography contains both $W_{F_3(p,q)}$ and $W_{\text{tw}+(S)}$ (and may contain more).

Thus, we obtain the result in Corollary 1.5:

$$\begin{aligned} g_T(T(2k, 2k-1)) &\geq \bar{\gamma}_3(T(2k, 2k-1)) \\ &\geq \bar{\gamma}_4(T(2k, 2k-1)) \\ &= k-1. \end{aligned}$$

We note that for $T(2k, 2k-1)$, it is not clear if $\hat{\gamma}_3^+ = \hat{\gamma}_4^+$; in fact, this seems unlikely to be the case, as the Seifert surface lies inside the wedge of the 3-dimensional pinch surface for $k > 1$.

5. ORDINARY GENUS GAPS: PRETZEL KNOTS

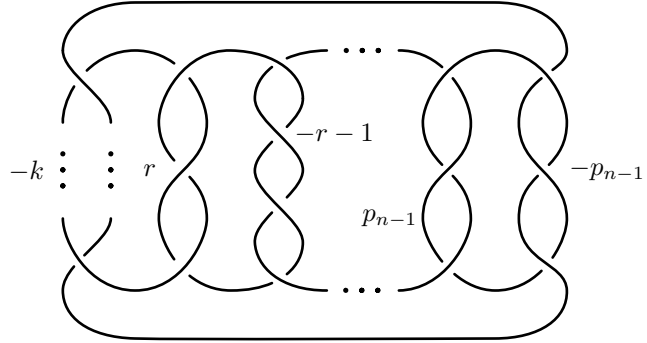
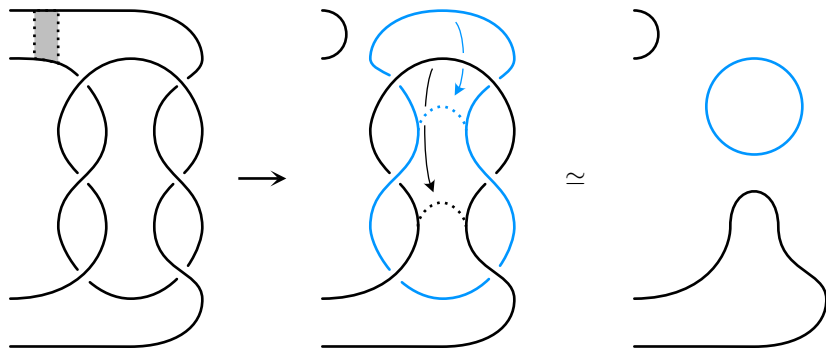
At the end of the previous section, we saw that the torus knot $T(4,3)$ has a gap of 1 between its non-orientable 3- and 4-genera. In fact, Jabuka and Van Cott [29] prove that the gap can be arbitrarily large on torus knots:

$$(\gamma_3(T(qk+1, q)) - \gamma_4(T(qk+1, q)) \geq \frac{k}{2}.$$

In this section, we provide a new family of examples for which the gap becomes arbitrarily large. These examples, which are a family of pretzel knots, have several interesting features. First, the new examples all bound Möbius bands in B^4 even though the orientable 4-genus becomes arbitrarily large. Second, the gap between the Euler-normalized non-orientable 3- and 4-genera is bounded above by 2, demonstrating that the Euler-normalized non-orientable gaps are independent of ordinary non-orientable gaps.

The main result of this section is Proposition 1.7, which asserts that for any $n \geq 1$ and positive odd integers $k, r, p_1, \dots, p_{n-1}$, the pretzel knot $P = P(-k, r, -r-1, p_1, -p_1, \dots, p_{n-1}, -p_{n-1})$ satisfies

- (1) $\gamma_4(P) = 1$,
- (2) $\gamma_3(P) = 2n$, and

FIGURE 14. The pretzel knot in Proposition 1.7 with $r = 3 = p_i$.FIGURE 15. A band move of Type I with $s = 3$.

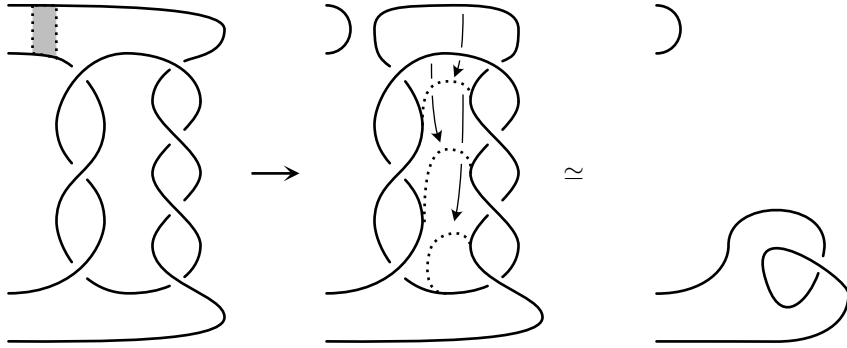
$$(3) \quad g_4(P) \geq \frac{1}{2}(k - r - 2).$$

Such a knot is illustrated in Figure 14 for $p_i = 3$.

Proof. The fact that $\gamma_3(P) = 2n$ follows directly from the work of Ichihara and Mizushima [27, Theorem 1.2].

To prove that $\gamma_4(P) = 1$, we begin by illustrating two types of band moves. A band move of Type I works for a pretzel of the form $P(q_1, \dots, q_{N-2}, s, -s)$ for $s \in \mathbb{Z}$ ($s \neq 0$). We can perform this band move between the twists q_{N-2} and s to obtain the pretzel $P(q_1, \dots, q_{N-2})$ and an unlinked unknot; see Figure 15. These band moves are always orientable, and show that $P(q_1, \dots, q_{N-2})$ and $P(q_1, \dots, q_{N-2}, s, -s)$ are concordant.

Next, consider a pretzel of the form $P(q_1, \dots, q_{N-2}, s, -(s+1))$ for $s \in \mathbb{Z}$ ($s \neq 0, -1$). A band move of Type II between q_{N-2} and s , pictured in Figure 16, reduces the knot to $P(q_1, \dots, q_{N-2})$. Note that this band move may be non-orientable.

FIGURE 16. A band move of Type II with $s = 3$.

We are now ready to prove that $\gamma_4(P) = 1$. Applying Type I moves $n - 1$ times, we see that P is concordant to $P(-k, r, -r - 1)$. A further band move of Type II (which is non-orientable) transforms $P(-k, r, -r - 1)$ into an unknot, and hence shows that P is filled by a Möbius band. Note that a diagrammatic computation using Equation (3.2) implies that the normal Euler number of the surface F constructed in this proof is

$$(5.1) \quad e(F) = 2(k - r - 1).$$

It remains to be shown that $g_4(P) \geq \frac{1}{2}(k - r - 2)$, which is achieved by calculating the signature of P . Since P is concordant to $P(-k, r, -r - 1)$, it suffices to compute the signature of the latter knot, which can be achieved either directly using the Goeritz matrix as in [19], or using the formulae for signatures of pretzel knots in [28] or [41] (correcting for sign conventions). The result is that:

$$(5.2) \quad \sigma(P) = \begin{cases} k - r & k < r(r + 1), \\ k - r - 2 & k > r(r + 1). \end{cases}$$

The lower bound for $g_4(P)$ now follows from applying Murasugi's signature bound [37]. \square

As mentioned at the beginning of this section, despite the large gaps between γ_3 and γ_4 for the knots in Proposition 1.7, these examples do not exhibit similarly large gaps between $\hat{\gamma}_3^\pm$ and $\hat{\gamma}_4^\pm$.

Proposition 5.1. *The pretzel knots P in Proposition 1.7 satisfy*

$$\hat{\gamma}_3^\pm(P) - \hat{\gamma}_4^\pm(P) \leq 2.$$

We conjecture that $\hat{\gamma}_3^\pm(P) - \hat{\gamma}_4^\pm(P) = 0$. The conjecture would hold if the Möbius band filling constructed in the proof of Proposition 1.7 were the unique such band.

Proof. Let F_A (resp. F_B) be the all- A (resp. all- B) state surface for P . Using Lemma 2.4, we compute that

$$e(F_A) = 2k + \sum_{i=1}^{n-1} p_i \quad \text{and} \quad e(F_B) = -4r - 2 - \sum_{i=1}^{n-1} p_i.$$

A direct computation on the diagram yields

$$b_1(F_A) = 2 + r + \sum_{i=1}^{n-1} p_i \quad \text{and} \quad b_1(F_B) = 1 + r + k + \sum_{i=1}^{n-1} p_i.$$

Putting these computations together with the formula for the signature of P in Equation (5.2) yields

$$\begin{aligned} \Gamma^-(F_A) &= \begin{cases} 2 & k < r(r+1) \\ 0 & k > r(r+1) \end{cases} \\ \Gamma^+(F_B) &= \begin{cases} 0 & k < r(r+1) \\ 2 & k > r(r+1) \end{cases} \end{aligned}$$

The proposition follows. \square

6. EULER-NORMALIZED GENUS GAPS: SLICE PRETZEL KNOTS

In this section, we prove Proposition 1.8 by exhibiting an infinite family of non-alternating slice pretzel knots with negative Euler-normalized non-orientable 3-genus 2. The techniques deployed in the proof are interesting more for their suggestion of what work would be necessary for the computation of the Euler-normalized genera of adequate knots and the proof of Conjecture 1.6 than for the result itself which, as noted above, would also follow from Theorems 1.3 and 1.4. The idea is reminiscent of the computation of the 3-dimensional geography of the trefoil (Example 2.5) and of the 5_2 knot (Example 2.6), but instead of using Adams and Kindred's idea that basic state surfaces "generate" the geography of alternating knots, we use instead the constraint on the geography coming from essential surfaces described in Proposition 2.10. That is, for pretzel knots, essential surfaces play the role that basic state surfaces play for alternating knots. This means that we need to understand all possible essential surfaces in the complement of a pretzel knot.

6.1. Essential Surfaces and Edgepath Systems. As a first step in the proof of Proposition 1.8, we describe the work of Hatcher and Oertel [23] on essential surfaces in the exteriors of Montesinos knots, specializing our description to the pretzel knots $P_n = P(-3, 3, n)$, with $n \geq 3$ odd, as in [26] or [33], when appropriate.

The central idea is that every essential surface belongs to a set \mathcal{C} of candidate surfaces that is constructed as follows. Suppose that K is a Montesinos knot composed of N rational tangles. Divide S^3 into N copies of B^3 that

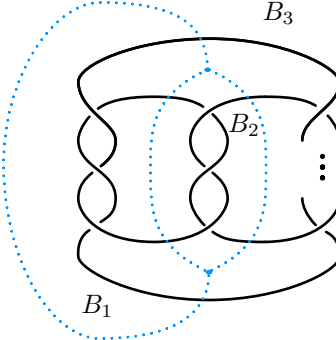


FIGURE 17. Divide S^3 into N copies of B^3 , with each tangle of K contained in its own 3-ball B_i . The two dots where the three B_i meet represent the points where the common S^1 axis meets the projection 2-sphere.

all meet along a common S^1 axis, with the k^{th} 3-ball containing the k^{th} tangle; see Figure 17. We produce candidate surfaces in \mathcal{C} by constructing subsurfaces that lie in the 3-balls and then ensuring that those subsurfaces match up along the common boundaries. The subsurfaces themselves are described by a sequence of saddles that is related to the twists that make up the rational tangles.

One of the insights of Hatcher and Oertel is that these subsurfaces can be described and analyzed using combinatorial data. The first step in the combinatorial description of a subsurface in a tangle is to record it as a path in the edgepath diagram $\mathcal{D} \subset \mathbb{R}^2$, with coordinates on \mathbb{R}^2 denoted (u, v) . The diagram \mathcal{D} consists of a collection of line segments with disjoint interiors that connect vertices of the form $\langle p/q \rangle = (1 - 1/q, p/q)$, $\langle p/q \rangle^\circ = (1, p/q)$, and $\langle 1/0 \rangle = (-1, 0)$ for $q > 1$, $p \in \mathbb{Z}$ and p and q relatively prime. There is a line segment joining $\langle p/q \rangle$ and $\langle r/s \rangle$ exactly when $ps - rq = \pm 1$; we denote such a line segment by $\langle p/q \rangle - \langle r/s \rangle$. The diagram \mathcal{D} also contains the horizontal segments $\langle p/q \rangle - \langle p/q \rangle^\circ$, and all segments $\langle 1/0 \rangle - \langle p/1 \rangle$; see Figure 18.

A **basic edgepath** $\tilde{\Lambda}$ describes a sequence of saddles in a tangle which must satisfy the following properties:

- (1) The path $\tilde{\Lambda}$ begins on the edge $\langle p/q \rangle - \langle p/q \rangle^\circ$, and is constant if the starting point is not $\langle p/q \rangle$.
- (2) The path $\tilde{\Lambda}$ proceeds monotonically from right to left, with movement along vertical edges permitted.
- (3) The path $\tilde{\Lambda}$ neither retraces itself nor travels along two edges of a triangle in \mathcal{D} in succession.

As noted in [27] or [33], it is straightforward to see that, for a pretzel knot, a basic edgepath takes one of the following two forms:

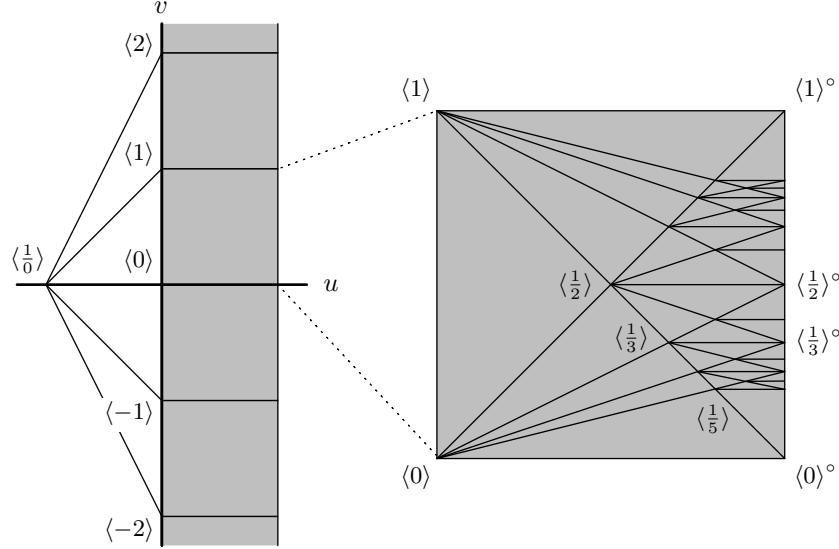


FIGURE 18. The edgepath diagram \mathcal{D} with the part of the diagram in $[0, 1] \times [0, 1]$ expanded.

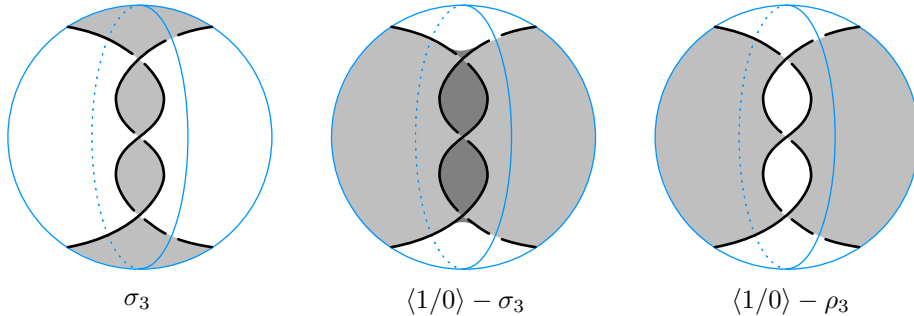


FIGURE 19. Examples of subsurfaces in a tangle corresponding to the edgepaths σ_3 , $\langle 1/0 \rangle - \sigma_3$, and $\langle 1/0 \rangle - \rho_3$. The longitudes represent the common axis of the 3-balls.

- (1) $\sigma_{\pm p} = \langle 0 \rangle - \langle \pm 1/p \rangle$
- (2) $\rho_{\pm p} = \langle \pm 1 \rangle - \langle \pm 1/2 \rangle - \cdots - \langle \pm 1/(|p|-1) \rangle - \langle \pm 1/|p| \rangle$

See Figure 19 for illustrations of surfaces corresponding to several basic edgepaths and their extensions to include the point $\langle 1/0 \rangle$. Note that an edgepath does not necessarily determine a unique subsurface, but it does uniquely determine the first Betti number and normal Euler number of a subsurface.

A **basic edgepath system** is simply a collection of basic edgepaths, one for each tangle. There are eight possible basic edgepath systems for the

pretzel knot P_n :

$$\begin{array}{ll} \tilde{\Lambda}_0 : \{\sigma_{-3}, \sigma_3, \sigma_n\} & \tilde{\Lambda}_4 : \{\rho_{-3}, \sigma_3, \sigma_n\} \\ \tilde{\Lambda}_1 : \{\sigma_{-3}, \sigma_3, \rho_n\} & \tilde{\Lambda}_5 : \{\rho_{-3}, \sigma_3, \rho_n\} \\ \tilde{\Lambda}_2 : \{\sigma_{-3}, \rho_3, \sigma_n\} & \tilde{\Lambda}_6 : \{\rho_{-3}, \rho_3, \sigma_n\} \\ \tilde{\Lambda}_3 : \{\sigma_{-3}, \rho_3, \rho_n\} & \tilde{\Lambda}_7 : \{\rho_{-3}, \rho_3, \rho_n\} \end{array}$$

In order to ensure that the edgepaths correspond to subsurfaces that match along their boundaries, we require that their (left) endpoints have the same u coordinate, and at that u value, the v coordinates sum to zero. In order to achieve this condition, we must extend or truncate basic edgepath systems in one of the following three ways:

Type I: Type I edgepath systems are formed by first extending basic edgepaths by appending an edge $\langle 1/p \rangle - \langle 1/p \rangle^\circ$. The extended system, which we shall continue to call $\tilde{\Lambda} = \{\tilde{\Lambda}_1, \dots, \tilde{\Lambda}_k\}$, can then be considered as a function $[0, 1] \rightarrow \mathbb{R}$ defined by $\tilde{\Lambda}(u) = \sum_{i=1}^k \tilde{\Lambda}_i(u)$. Solve the equation $\tilde{\Lambda}(u) = 0$. For each solution u_0 , a new Type I edgepath system Λ with edgepaths Λ_i is constructed according to the following algorithm: if $u_0 \leq (|p_i| - 1)/|p_i|$, then let

$$\Lambda_i = \tilde{\Lambda}_i \cap \{(u, v) : u \geq u_0\}.$$

This procedure may cut an edge in its interior. Denote such a partial edge on $\langle p/q \rangle - \langle r/s \rangle$ by

$$\left(\frac{k}{k+l} \langle p/q \rangle - \frac{l}{k+l} \langle r/s \rangle \right) - \langle r/s \rangle,$$

where $k + l$ is the number of sheets of the surface, and

$$u_0 = \frac{k(q-1) + l(s-1)}{kq + ls}.$$

See [23, p. 455].

Type II: Add vertical edges to edgepaths in $\tilde{\Lambda}$ so that the v -coordinates of the endpoints sum to 0 when $u = 0$, while still adhering to the rule that an edgepath must not trace two sides of the same triangle. Only the minimal number of vertical edges need be added, as any additional pairs of edges will raise the first Betti number without changing the boundary slope.

Type III: Complete each basic edgepath with a segment connecting the left endpoint to $\langle 1/0 \rangle$.

The result of any one of these operations is an **edgepath system** Λ .

We are now in a position to enumerate all possible edgepath systems that describe surfaces in the candidate set \mathcal{C} for the pretzel knot P_n . According to the proof of Lemma 3.7 in [27], there is a unique Type I edgepath system

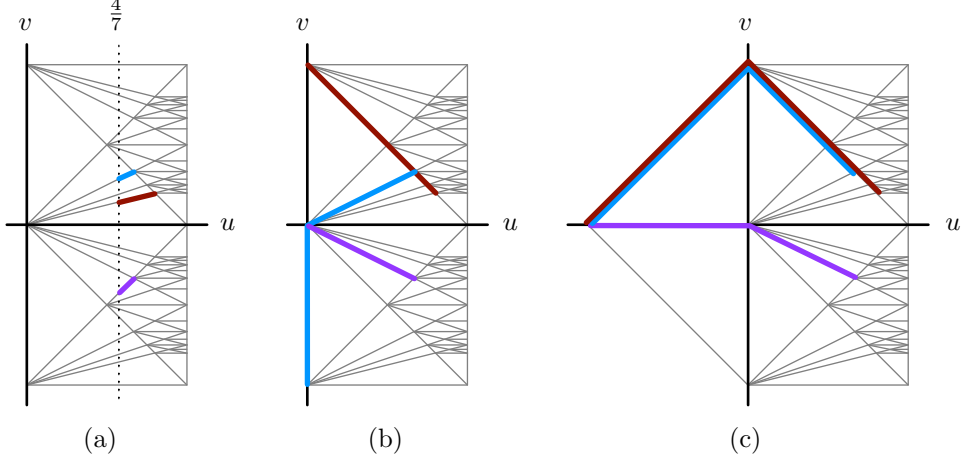


FIGURE 20. (a) The edgepath system Λ^I , (b) the edgepath system Λ_1^{II} , and (c) the edgepath system Λ_3^{III} , all with $n = 5$.

of the form

$$\Lambda^I = \left\{ \begin{array}{l} \left(\frac{4}{n+1} \langle -\frac{1}{2} \rangle + \frac{n-3}{n+1} \langle -\frac{1}{3} \rangle \right) - \langle -\frac{1}{3} \rangle, \\ \left(\frac{2}{n+1} \langle 0 \rangle + \frac{n-1}{n+1} \langle \frac{1}{3} \rangle \right) - \langle \frac{1}{3} \rangle, \\ \left(\frac{n-1}{n+1} \langle 0 \rangle + \frac{2}{n+1} \langle \frac{1}{n} \rangle \right) - \langle \frac{1}{n} \rangle \end{array} \right\}$$

See Figure 20(a) for an illustration of this system.

To specify Type II edgepath systems, we use a superscript + (resp. -) to denote the addition of an upward-pointing (resp. downward-pointing) vertical edge. In some cases, there are choices about where to attach a vertical edge, but such choices will be immaterial to later computations of the first Betti number and the normal Euler number. Up to such choices, the Type II edgepath systems are as follows:

$$\begin{array}{ll} \Lambda_0^{II} : \{\sigma_{-3}, \sigma_3, \sigma_n\} & \Lambda_4^{II} : \{\rho_{-3}, \sigma_3^+, \sigma_n\} \\ \Lambda_1^{II} : \{\sigma_{-3}, \sigma_3^-, \rho_n\} & \Lambda_5^{II} : \{\rho_{-3}, \sigma_3, \rho_n\} \\ \Lambda_2^{II} : \{\sigma_{-3}, \rho_3, \sigma_n^-\} & \Lambda_6^{II} : \{\rho_{-3}, \rho_3, \sigma_n\} \\ \Lambda_3^{II} : \{\sigma_{-3}^{--}, \rho_3, \rho_n\} & \Lambda_7^{II} : \{\rho_{-3}^-, \rho_3, \rho_n\} \end{array}$$

The edgepath system Λ_0^{II} corresponds to the Seifert surface of P_n . See Figure 20(b) for an illustration of a different Type II system, and see Figure 21(a) for an illustration of the Seifert surface.

Finally, Type III edgepath systems build directly off of the basic edgepath systems; we denote them by Λ_k^{III} for $k = 0, \dots, 7$. See Figure 20(c) for one example of a Type III edgepath system, and see Figure 21(b,c,d) for illustrations of surfaces that correspond to Type III edgepath systems.

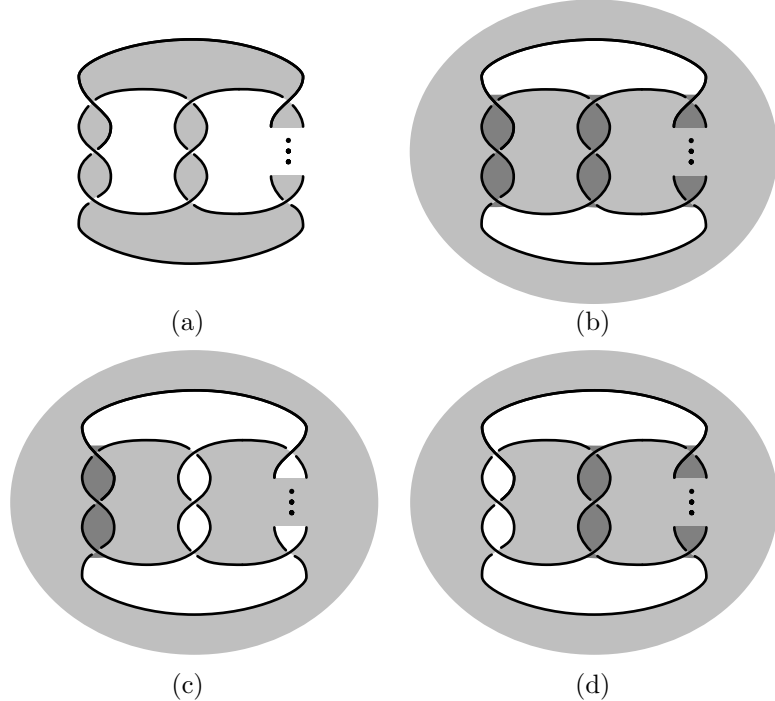


FIGURE 21. Spanning surfaces corresponding to several edgepath systems: (a) the Seifert surface Λ_0^{II} , (b) the surface Λ_0^{III} , (c) the all- A surface Λ_3^{III} , and (d) the all- B surface Λ_4^{III} .

6.2. Computations on Edgepath Systems. Now that we know how to construct edgepath systems that describe candidate surfaces, we proceed to describe how to compute the first Betti number and the normal Euler number of those candidates from their edgepath systems. We continue to follow [23, 26, 33].

We first define several quantities related to an edge in an edgepath.

- The **length** $|e|$ of an edge e is 1 for a complete edge between two vertices, and is $\frac{k}{k+l}$ for a partial edge $\left(\frac{k}{k+l}\langle p/q \rangle + \frac{l}{k+l}\langle r/s \rangle\right) - \langle r/s \rangle$. The length $|\Lambda|$ of an edgepath system is the sum of the lengths of its constituent edges that lie in the half-plane $u \geq 0$.
- The **sign** $\varepsilon(e)$ of an edge e is $+1$ if the edge increases in height from right to left, or is an upward-pointing vertical edge, and is -1 if the edge decreases in height from right to left, or is a downward-pointing vertical edge. The sign of the edge $e = \langle p/q \rangle - \langle r/s \rangle$ can also be computed as $\varepsilon(e) = ps - qr$.
- The **twist** $\tau(e)$ of an edge e is $\tau(e) = -2\varepsilon(e)|e|$ if e lies in the right half-plane $u \geq 0$, and $\tau(e) = 0$ if e connects an integer point $\langle n/1 \rangle$ to

$\langle 1/0 \rangle$. The twist $\tau(\Lambda)$ of an edgepath system is the sum of the twists of its constituent edges; as with the length, this is equivalent to the sum of the twists of its constituent edges that lie in the half-plane $u \geq 0$.

The computation of the Euler characteristic of a surface corresponding to an edgepath system depends on its type, and further, on the number of sheets $\#\Lambda$ of the surface described by the edgepath system. For Type II and Type III surfaces, we may assume for our purposes that the number of sheets is always one, but the Type I surfaces can have multiple sheets.

Type I: For a Type I edgepath system with N subsurfaces, $\#\Lambda$ sheets, and left endpoint at u_0 , we have

$$\frac{\chi(\Lambda)}{\#\Lambda} = -|\Lambda| + N - \frac{1}{1-u_0}(N-2).$$

Type II: For a Type II edgepath system, we have

$$\chi(\Lambda) = 2 - |\Lambda|.$$

Type III: For a Type III edgepath system, we have

$$\chi(\Lambda) = -|\Lambda|.$$

For the Type I edgepath system, we may calculate that $u_0 = \frac{2n-2}{3n-1}$ and that the associated surface has $\frac{n+1}{2}$ sheets; the division by 2 arises since the fractions in Λ^I have even numerators and denominators since n is odd, so the denominator in lowest terms is $\frac{n+1}{2}$. Further, the three edgepaths have lengths $\frac{4}{n+1}$, $\frac{2}{n+1}$, and $\frac{n-1}{n+1}$. The formula above then yields $\chi(\Lambda^I) = -\frac{n+1}{2}$, so $b_1(\Lambda^I) = \frac{n+3}{2}$. The calculations of the first Betti numbers of the Type II and Type III appear in the third columns of Table 1(a) and (b), respectively.

The computation for the boundary slope is similar, though simpler. Denote the edgepath system corresponding to the Seifert surface of P_n by Λ_S . For a surface corresponding to the edgepath Λ , we have

$$s(\Lambda) = \tau(\Lambda) - \tau(\Lambda_S),$$

and hence

$$e(\Lambda) = \tau(\Lambda_S) - \tau(\Lambda).$$

As noted above, the Seifert surface corresponds to Λ_0^{II} , which has twist 2. For the Type I edgepath system, all three edgepaths have negative signs, and hence we obtain $e(\Lambda^I) = -\frac{8}{n+1}$. See Table 1 once again for the normal Euler numbers of the Type II and Type III surfaces.

We now have enough information for the proof of Proposition 1.8.

Proof of Proposition 1.8. The point of Hatcher and Oertel's algorithm is that every essential surface corresponds to one of the Type I, II, or III edgepath systems.

The calculations above show that the Type I surface has $\Gamma^-(\Lambda^I) = \frac{n+2}{2} - \frac{4}{n+1}$. For odd $n \geq 3$, we have $\Gamma^-(\Lambda^I) \geq \frac{3}{2}$. Thus, any spanning surface that

Λ_k^{II}	e	b_1	Γ^+	Γ^-	Λ_k^{III}	e	b_1	Γ^+	Γ^-
(0)	0	2	2	2	(0)	0	4	4	4
(1)	$2n - 2$	$n + 1$	2	$2n$	(1)	$2n$	$n + 2$	2	$2n + 2$
(2)	4	4	2	6	(2)	6	5	2	8
(3)	$2n + 2$	$n + 3$	2	$2n + 4$	(3)	$2n + 6$	$n + 3$	0	$2n + 6$
(4)	-4	4	6	2	(4)	-6	5	8	2
(5)	$2n - 6$	$n + 1$	4	$2n - 2$	(5)	$2n - 6$	$n + 3$	6	$2n$
(6)	0	4	4	4	(6)	0	6	6	6
(7)	$2n - 2$	$n + 3$	4	$2n + 2$	(7)	$2n$	$n + 4$	4	$2n + 4$

TABLE 1. First Betti numbers, normal Euler numbers, and Γ computations for (a) Type II edgepath systems and (b) Type III edgepath systems. Minimal values of Γ^\pm are boxed.

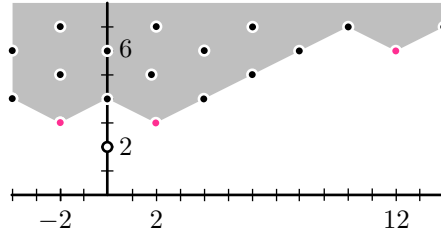


FIGURE 22. The 3-dimensional geography of the knot P_3 is generated by the all- A state surface at $(12, 6)$ and the positively and negatively twisted Seifert surface at $(\pm 2, 3)$. The Type I surface also lies at $(-2, 3)$.

boundary compresses to the surface corresponding to Λ^I must have $\Gamma^-(F) \geq 2$. Further, Table 1 shows that Γ^- is at least 2 for each of the Type II and Type III surfaces. Thus, Corollary 2.12 shows that $\hat{\gamma}_3^-(P_n) \geq 2$. On the other hand, the all- B surface corresponding to Λ_k^{III} yields $\hat{\gamma}_3^+(P_n) = 0$. \square

Example 6.1. The information generated for the proof of Proposition 1.8 also yields, via Proposition 2.10, the geography of the knots P_n . See Figure 22 for the geography of P_3 .

Remark 6.2. Hatcher and Oertel's algorithm goes further than just listing candidates the essential surfaces in the exterior of a Montesinos knot — it can actually identify which of these are essential. We chose not to use

this part of Hatcher and Oertel's work since the combinatorics necessary to pick out the essential surfaces from the candidates were more involved than simply computing the normal Euler and Betti numbers for all of the candidates. Nevertheless, computations using Dunfield's implementation of Hatcher and Oertel's algorithm [13] indicates that the essential surfaces for P_n correspond to the edgepath systems Λ^I , Λ_0^{II} (the Seifert surface), Λ_0^{III} , and Λ_3^{III} (the all- B surface).

7. EULER-NORMALIZED GENUS GAPS: CONNECTED SUMS

We conclude by investigating the behavior of the Euler-normalized non-orientable genus under connected sum. In particular, we prove the additivity of the Euler-normalized non-orientable 3-genus. The proof of Theorem 1.9 will follow as an immediate corollary.

Lemma 7.1. *The Euler-normalized non-orientable 3-genera $\hat{\gamma}_3^\pm$ are each additive under connected sum, i.e.*

$$\hat{\gamma}_3^\pm(K_0 \# K_1) = \hat{\gamma}_3^\pm(K_0) + \hat{\gamma}_3^\pm(K_1).$$

The proof of the lemma is, in essence, the same as the proof of subadditivity of the non-orientable 3-genus in [9, Theorem 2.8] with two important differences:

- (1) The need to track the normal Euler number, and
- (2) The freedom to add twisted bands to move off of the orientable spanning surfaces that force subadditivity rather than additivity of the ordinary non-orientable 3-genus.

In the proof below, we use the standard notation that if F_i is a spanning surface for K_i , then $F_0 \natural F_1$ is the boundary connected sum of F_0 and F_1 , with $\partial(F_0 \natural F_1) = K_0 \# K_1$.

Proof. We write the proof in the positive case; the negative case is analogous. Let F be a non-orientable spanning surface for $K_0 \# K_1$ that realizes $\hat{\gamma}_3^+(K_0 \# K_1)$.

Using standard arguments (see, for example, [14, §5]), we may decompose F as $F_0 \natural F_1$, where F_i is a spanning surface for K_i . If F realizes $\hat{\gamma}_3^+(K_0 \# K_1)$, then so does $\text{tw}_+^k(F)$, the surface obtained from the addition of k positive twisted bands. Thus, we may assume that the surfaces F_i are non-orientable. It suffices to prove that, for $i = 0, 1$, we have $\hat{\gamma}_3^+(K_i) = \Gamma^+(F_i)$.

Suppose, to the contrary, that there exists a spanning surface F_0^* of K_0 so that

$$(7.1) \quad \Gamma^+(F_0^*) < \Gamma^+(F_0).$$

If $e(F_0^*) \leq e(F_0)$, then add $k = e(F_0) - e(F_0^*)$ positive twisted bands to F_0^* , yielding a surface $\text{tw}_+^k(F_0^*)$ with $e(\text{tw}_+^k(F_0^*)) = e(F_0)$. As adding twisted bands does not change Γ^+ , Equation (7.1) shows that $b_1(\text{tw}_+^k(F_0^*)) < b_1(F_0)$. It follows that $b_1(\text{tw}_+^k(F_0^*) \natural F_1) < b_1(F)$. Since $\text{tw}_+^k(F_0^*) \natural F_1$ and F have the

same normal Euler number, we see that $\Gamma^+(\text{tw}_+^k(F_0^*) \# F_1) < \Gamma^+(F)$. This contradicts the assumption that F realizes $\hat{\gamma}_3^+(K_0 \# K_1)$.

If, on the other hand, $e(F_0^*) > e(F_0)$, we add twisted bands to F_0 so that $e(\text{tw}_+^k(F_0)) = e(F_0^*)$. A parallel argument to the one above once again leads to the required contradiction. \square

Proof of Theorem 1.9. As in Section 6, consider the pretzel knot $P = P(-3, 3, 3)$. We know that $\hat{\gamma}_3^-(P) = 2$, while $\hat{\gamma}_4^-(P) = 0$ since P is slice. Let $K_n = \#_n P$. On one hand, Lemma 7.1 shows that $\hat{\gamma}_3^-(K_n) = 2n$. On the other, the knot K_n is slice, so $\hat{\gamma}_4^-(K_n) = 0$. The theorem follows. \square

REFERENCES

1. Tetsuya Abe and Kengo Kishimoto, *The dealternating number and the alternation number of a closed 3-braid*, J. Knot Theory Ramifications **19** (2010), no. 9, 1157–1181. MR 2726563
2. Colin Adams and Thomas Kindred, *A classification of spanning surfaces for alternating links*, Algebr. Geom. Topol. **13** (2013), no. 5, 2967–3007. MR 3116310
3. Samantha Allen, *Nonorientable surfaces bounded by knots: a geography problem*, New York J. Math. **29** (2023), 1038–1059. MR 4646147
4. William Ballinger, *Concordance invariants from the $e(-1)$ spectral sequence on khovanov homology*, Preprint available as arXiv:2004:10807, 2020.
5. Joshua Batson, *Nonorientable slice genus can be arbitrarily large*, Math. Res. Lett. **21** (2014), no. 3, 423–436. MR 3272020
6. Fraser Binns, Sungkyung Kang, Jonathan Simone, and Paula Truöl, *On the nonorientable four-ball genus of torus knots*, Preprint available as arXiv:2109.09187, 2021.
7. Benjamin A. Burton and Melih Ozlen, *Computing the crosscap number of a knot using integer programming and normal surfaces*, ACM Trans. Math. Software **39** (2012), no. 1, Art. 4, 18. MR 3002773
8. Abhijit Champanerkar and Ilya Kofman, *A survey on the Turaev genus of knots*, Acta Math. Vietnam. **39** (2014), no. 4, 497–514. MR 3292579
9. Bradd Evans Clark, *Crosscaps and knots*, Internat. J. Math. Math. Sci. **1** (1978), no. 1, 113–123. MR 478131
10. Cynthia L. Curtis and Samuel J. Taylor, *The Jones polynomial and boundary slopes of alternating knots*, J. Knot Theory Ramifications **20** (2011), no. 10, 1345–1354. MR 2851712
11. Aliakbar Daemi and Christopher Scaduto, *Chern–Simons functional, singular instantons, and the four-dimensional clasp number*, J. Eur. Math. Soc. (JEMS) **26** (2024), no. 6, 2127–2190. MR 4742808
12. Oliver T. Dasbach, David Futer, Efstratia Kalfagianni, Xiao-Song Lin, and Neal W. Stoltzfus, *The Jones polynomial and graphs on surfaces*, J. Combin. Theory Ser. B **98** (2008), no. 2, 384–399. MR 2389605
13. Nathan M. Dunfield, *Boundary slopes of Montesinos knots*, URL: <https://github.com/NathanDunfield/montesinos>, 2020.
14. Ralph H. Fox, *A quick trip through knot theory*, Topology of 3-manifolds and related topics (Proc. The Univ. of Georgia Institute, 1961), Prentice-Hall, Inc., Englewood Cliffs, NJ, 1961, pp. 120–167. MR 140099
15. David Futer, Efstratia Kalfagianni, and Jessica S. Purcell, *Slopes and colored Jones polynomials of adequate knots*, Proc. Amer. Math. Soc. **139** (2011), no. 5, 1889–1896. MR 2763776
16. Stavros Garoufalidis, *The Jones slopes of a knot*, Quantum Topol. **2** (2011), no. 1, 43–69. MR 2763086

17. Patrick M. Gilmer and Charles Livingston, *The nonorientable 4-genus of knots*, J. Lond. Math. Soc. (2) **84** (2011), no. 3, 559–577. MR 2855790
18. Marco Golla and Marco Marengon, *Correction terms and the nonorientable slice genus*, Michigan Math. J. **67** (2018), no. 1, 59–82. MR 3770853
19. Cameron McA. Gordon and Richard A. Litherland, *On the signature of a link*, Invent. Math. **47** (1978), no. 1, 53–69. MR 500905
20. Joshua Greene and Stanislav Jabuka, *The slice-ribbon conjecture for 3-stranded pretzel knots*, Amer. J. Math. **133** (2011), no. 3, 555–580. MR 2808326
21. Joshua Evan Greene, *Alternating links and definite surfaces*, Duke Math. J. **166** (2017), no. 11, 2133–2151, With an appendix by András Juhász and Marc Lackenby. MR 3694566
22. Allen Hatcher, *On the boundary curves of incompressible surfaces*, Pacific J. Math. **99** (1982), no. 2, 373–377. MR 658066
23. Allen Hatcher and Ulrich Oertel, *Boundary slopes for Montesinos knots*, Topology **28** (1989), no. 4, 453–480. MR 1030987
24. Allen Hatcher and William Thurston, *Incompressible surfaces in 2-bridge knot complements*, Invent. Math. **79** (1985), no. 2, 225–246. MR 778125
25. Mikami Hirasawa and Masakazu Teragaito, *Crosscap numbers of 2-bridge knots*, Topology **45** (2006), no. 3, 513–530. MR 2218754
26. Kazuhiro Ichihara and Shigeru Mizushima, *Bounds on numerical boundary slopes for Montesinos knots*, Hiroshima Math. J. **37** (2007), no. 2, 211–252. MR 2345368
27. ———, *Crosscap numbers of pretzel knots*, Topology Appl. **157** (2010), no. 1, 193–201. MR 2556097
28. Stanislav Jabuka, *Rational Witt classes of pretzel knots*, Osaka J. Math. **47** (2010), no. 4, 977–1027. MR 2791566
29. Stanislav Jabuka and Cornelia A. Van Cott, *Comparing nonorientable three genus and nonorientable four genus of torus knots*, J. Knot Theory Ramifications **29** (2020), no. 3, 2050013, 15. MR 4101607
30. ———, *On a nonorientable analogue of the Milnor conjecture*, Algebr. Geom. Topol. **21** (2021), no. 5, 2571–2625. MR 4334520
31. Efstratia Kalfagianni, *A Jones slopes characterization of adequate knots*, Indiana Univ. Math. J. **67** (2018), no. 1, 205–219. MR 3776020
32. ———, *State surfaces of links*, Encyclopedia of Knot Theory (Colin Adams, Erica Flapan, Allison Henrich, Louis H. Kauffman, Lewis D. Ludwig, and Sam Nelson, eds.), CRC Press, 2021.
33. Christine Ruey Shan Lee and Roland van der Veen, *Slopes for pretzel knots*, New York J. Math. **22** (2016), 1339–1364. MR 3576292
34. Charles Livingston and Allison H. Moore, *Knotinfo: Table of knot invariants*, URL: knotinfo.org, December 2025.
35. Adam Lowrance, *The Khovanov width of twisted links and closed 3-braids*, Comment. Math. Helv. **86** (2011), no. 3, 675–706. MR 2803857
36. William S. Massey, *Proof of a conjecture of Whitney*, Pacific Journal of Mathematics **31** (1969), no. 1, 143 – 156.
37. Kunio Murasugi, *On a certain numerical invariant of link types*, Trans. Amer. Math. Soc. **117** (1965), 387–422. MR 171275
38. Peter S. Ozsváth, András I. Stipsicz, and Zoltán Szabó, *Unoriented knot Floer homology and the unoriented four-ball genus*, Int. Math. Res. Not. IMRN (2017), no. 17, 5137–5181. MR 3694597
39. Joshua M. Sabloff, *On a refinement of the non-orientable 4-genus of torus knots*, Proc. Amer. Math. Soc. Ser. B **10** (2023), 242–251. MR 4604871
40. Kouki Sato, *An unoriented analogue of slice-torus invariant*, Preprint available as arXiv:2404.04056, 2024.

41. Yaichi Shinohara, *On the signature of pretzel links*, Topology and computer science (Atami, 1986), Kinokuniya, Tokyo, 1987, pp. 217–224. MR 1112594
42. Masakazu Teragaito, *Crosscap numbers of torus knots*, Topology Appl. **138** (2004), no. 1-3, 219–238. MR 2035482
43. Paweł Traczyk, *A combinatorial formula for the signature of alternating diagrams*, Fund. Math. **184** (2004), 311–316. MR 2128055
44. Oleg Ja. Viro, *Positioning in codimension 2, and the boundary*, Uspehi Mat. Nauk **30** (1975), no. 1(181), 231–232. MR 0420641
45. Akira Yasuhara, *Connecting lemmas and representing homology classes of simply connected 4-manifolds*, Tokyo J. Math. **19** (1996), no. 1, 245–261. MR 1391941

HAVERFORD COLLEGE, HAVERFORD, PA 19041

Email address: jknihs0401@gmail.com

HAVERFORD COLLEGE, HAVERFORD, PA 19041

Email address: jpatel@haverford.edu

CORNELL UNIVERSITY, ITHACA, NY 14853

Email address: dgr77@cornell.edu

HAVERFORD COLLEGE, HAVERFORD, PA 19041

Email address: jsabloff@haverford.edu